State Preparation and Excited Electronic and Vibrational Behavior in Hemes†

J. Reddy Challa, Tissa C. Gunaratne, and M. Cather Simpson*

Center for Chemical Dynamics, Department of Chemistry, Case Western Reserve University, Cleveland, Ohio 44106

Received: June 7, 2006; In Final Form: August 14, 2006

The temporally overlapping, ultrafast electronic and vibrational dynamics of a model five-coordinate, high-spin heme in a nominally isotropic solvent environment has been studied for the first time with three complementary ultrafast techniques: transient absorption, time-resolved resonance Raman Stokes, and time-resolved resonance Raman anti-Stokes spectroscopies. Vibrational dynamics associated with an evolving ground-state species dominate the observations. Excitation into the blue side of the Soret band led to very rapid $S_2 \rightarrow S_1$ decay (sub-100 fs), followed by somewhat slower (800 fs) $S_1 \rightarrow S_0$* nonradiative decay. The initial vibrationally excited, non-Boltzmann S_0* state was modeled as shifted to lower energy by 300 cm^{-1} and broadened by 20%. On a ∼10 ps time scale, the S_0* state evolved into its room-temperature, thermal distribution S_0 profile largely through VER. Anti-Stokes signals disappear very rapidly, indicating that the vibrational energy redistributes internally in about 1−3 ps from the initial accepting modes associated with $S_1 \rightarrow S_0$ internal conversion to the rest of the macrocycle. Comparisons of anti-Stokes mode intensities and lifetimes from TRARRS studies in which the initial excited state was prepared by ligand photolysis [Mizutani, T.; Kitagawa, T. *Science* **1997**, *278*, 443, and *Chem. Rec.* **2001**, *1*, 258] suggest that, while transient absorption studies appear to be relatively insensitive to initial preparation of the electronic excited state, the subsequent vibrational dynamics are not. Direct, time-resolved evaluation of vibrational lifetimes provides insight into fast internal conversion in hemes and the pathways of subsequent vibrational energy flow in the ground state. The overall similarity of the model heme electronic dynamics to those of biological systems may be a sign that the protein's influence upon the dynamics of the heme active site is rather subtle.

Introduction

Metalloporphyrins (MPs), particularly hemes, constitute an important class of molecules whose prevalence in biology and increasingly realized potential for technological applications such as fuel cells and photodetoxificants makes understanding their photodynamics essential. Despite more than 20 years of active research by several groups, the understanding of the electronic and vibrational behavior of photoexcited hemes has still not converged to a single model. There is some consensus, however.[1−17] Photoexcitation into the strong Soret ($\pi-\pi^*$) transition of the heme group leads to rapid internal conversion (IC) that deposits a large excess of vibrational energy in the ground electronic state within 5 ps. The dynamics apparently remain within the singlet manifold of the heme. The remaining questions surrounding the events that occur within this short but crucial time interval concern the possibility of intervening electronic states and their characteristics and lifetimes.

The vibrational manifolds of these states, both ground and excited, are important contributors to fast heme dynamics. The redistribution of vibrational energy in molecules undergoing chemical reactions and/or responding to photoexcitation is a fundamental process that may significantly influence reactivity, yet is not well-understood. In the condensed phase, this flow can be separated phenomenologically into two components: *intra*molecular vibrational energy redistribution (IVR) among the modes of the molecule and *inter*molecular vibrational energy relaxation (VER) from the molecule to the solvent. In general, the time scales of IVR and VER overlap, often presenting a rather complex picture. In hemes, the very fast electronic IC processes complicate experimental observations further, both via mode-selective facilitation that gives rise to a non-Boltzmann vibrational energy distribution on the lower-energy state and by overlapping temporally with the vibrational dynamics themselves. Assigning the contributions of IVR, VER, and electronic dynamics to the observed behavior presents a formidable challenge.

The subnanosecond dynamics of hemes have been investigated using transient and time-resolved spectroscopies.[1−17] The rapid IC back to the ground state in less than 5 ps is followed by a return to thermal equilibrium through IVR among the porphyrin modes and VER to the protein/solvent. Reported IVR rates vary from about 1.5 to 10 ps,[1,2,9−18] while the "global" lifetime associated with cooling is on the order of 5−40 ps.[7−10,16,19−22] Among the more interesting reports is the implication that mode-selective energy dissipation plays a significant role in directing heme biochemical reactions.[23−26] Intriguing recent computational studies indicate that the relative importance of "through-space" and "through-bond" dissipation of excess kinetic energy from the heme to the protein is protein-dependent.[22,27,28]

Unfortunately, much of what is experimentally determined about vibrational energy flow in hemes is inferential, derived from the interpretation of evolving line shapes observed in transient absorption spectra[2−8] or from transient Raman experiments using nanosecond pulses.[9−13] Despite the interest in, and

† Part of the special issue "Charles B. Harris Festschrift".

* Corresponding author. M. Cather Simpson. Department of Chemistry, Clapp Hall, Case Western Reserve University, Cleveland, OH 44022-7078. Fax: (216) 368-3006. E-mail: mcs9@po.cwru.edu.

10.1021/jp063543p CCC: $33.50
Published on Web 09/12/2006

fundamental importance of, heme vibrational dynamics, only a few direct studies have been reported, and a number of these are complicated by ligand photolysis dynamics that occur on the same time scale.

The most direct approach to studying vibrational dynamics is ultrafast pump−probe spectroscopy in which the probe is incoherent anti-Stokes Raman scattering (see, for example, refs 29−32). Anti-Stokes and Stokes Raman intensities are proportional to different vibrational-state subpopulations: Anti-Stokes only occurs from $v > 0$ vibrational levels, while Stokes is generated by all levels, including $v = 0$. Thus, the time dependence of anti-Stokes signals can, in theory, yield quantitative vibrational population dynamics. The direct, ultrafast experiment employs a short pump pulse to excite the system, followed by a visible probe pulse to interrogate the anti-Stokes intensities by taking snapshots of the anti-Stokes spectrum as a function of delay time. When the pump pulse is in the UV−vis region of the spectrum, the vibrational excitation on the ground electronic state is generated by rapid IC of the initial electronic excited state back to S_0. The time-dependent integrated intensities, positions, and line shapes thus reflect important information about vibrational coupling in IC and the time dependence of vibrational energy disposal in the ground state.

This method has been employed by us to study heme vibrational dynamics directly, and initial results are reported here. Ultrafast, time-resolved, UV−vis pump−anti-Stokes resonance Raman probe spectroscopy (TRARRS) was used to probe the vibrational dynamics of a model compound for deoxyhemoglobin: Fe^{II} octaethyl porphyrin with a 2-methyl imidazole ligand (FeOEP−2MeIm) in CH_2Cl_2. The system was both excited and probed in the Soret $\pi-\pi^*$ (S_2) transition in a one-color configuration. To tease out the electronic and vibrational contributions to the observed dynamics, parallel ultrafast, time-resolved UV−vis pump−Stokes resonance Raman probe (TR^3S) and ultrafast transient absorption (TA) spectroscopy were employed in the Soret region of the UV−vis spectrum as well. The results are compared to similar studies involving ligand photolysis in heme proteins from the perspective of state preparation effects upon IC and the subsequent vibrational dynamics.

To the best of our knowledge, this study is the first detailed ultrafast dynamical investigation of the biologically important, 5-coordinate, high-spin heme complex in the absence of the highly anisotropic protein environment. The potential impact of the protein upon heme dynamics includes effects upon the UV−vis static and dynamic line shapes, the excited electronic-state decay pathways and lifetimes, and the flow of vibrational energy within the heme (IVR) and out of the heme to the environment (VER). Thus, the results presented here are also discussed in terms of the insight they provide into the influence of the protein upon the heme active site dynamics.

Materials and Methods

Sample Preparation. $Iron^{II}$ octaethyl porphyrin 2-methyl imidazole (Fe^{II}OEP−2MeIm) was prepared with a two-phase approach.[11] All solutions were degassed and kept under slight N_2(g) overpressure during sample preparation and experimental interrogation. 2-Methyl imidazole (2MeIm; Aldrich) was recrystallized at least twice from benzene. Fe^{III}OEP (Porphyrin Products; no further purification) was dissolved in CH_2Cl_2 (Fisher; spectroscopic grade) at a concentration of 0.5−1.0 mM. Ten milliliters of this solution was added to an equal volume of CH_2Cl_2 saturated with 2MeIm, thereby diluting the porphyrin by a factor of 2. Then, 10 mL of 1.0 M $Na_2S_2O_4$ in deionized, distilled water and saturated with 2MeIm was added to the Fe^{III}OEP/2MeIm in CH_2Cl_2 solution under nitrogen pressure using an airtight syringe (Hamilton). Note that the porphyrin is not diluted by this addition; CH_2Cl_2 is poorly miscible with water, and the two phases remain distinct. The aqueous phase (contains ligand and reducing agent) is less dense than the CH_2Cl_2 phase (contains porphyrin and ligand).

To reduce the iron, the two phases are mixed by agitation. The formation of Fe^{II}OEP−2MeIm has been measured using UV−vis spectroscopy and is routinely monitored by the deep red color of the porphyrin solution and the position and shape of ν_4 in the Stokes spectrum. After the layers separate, the top (aqueous) layer contains excess ligand and reducing agent and acts as a protective barrier toward oxygen diffusion into porphyrin-containing CH_2Cl_2 layer below; this enhances the redox stability of the sample. When flowing the sample during experiments, only the more dense, porphyrin-containing layer is circulated.

Ultrafast Time-Resolved Resonance Raman Spectroscopy. The details of the laser system used for time-resolved resonance Raman studies has been described elsewhere.[33] Briefly, the output of a Ti:sapphire-based regenerative amplifier (785−835 nm, 120 fs, 650 ± 50 μJ/pulse, 1 kHz; Clark MXR, Inc.) was frequency-doubled in a long (30 mm) KDP crystal to produce 410 or 413 nm pulses (17−25 cm^{-1} fwhm, 500−800 fs, 60−70 μJ/pulse). A 50−50 beam splitter generated pump and probe beams, which were attenuated to 5.5 and 2.5 μJ/pulse, respectively, using neutral density filters. The probe beam, after passing through a motorized, calibrated translational stage (MM3000; Newport Inc.), was overlapped with the pump beam at the sample in a nearly collinear (∼5°) geometry with a spot size of ∼2 mm at the sample. This relatively large spot size was necessary to ensure an absence of sample degradation during the experiment. The sample was flowed through a 1 mm flow cell using Teflon tubing and an overpressure of N_2(g). Care was taken to flow only the denser, organic layer containing the Fe^{II}OEP−2MeIm.

Raman spectra were collected in a ∼135° backscattering geometry. Rayleigh scatter was rejected with an angle-tuned supernotch filter (center $\lambda = 415$ nm; Kaiser, Inc.). The Raman scattering was dispersed with a 0.5 m imaging spectrograph (500 is, Chromex, Inc.) and recorded with a thermoelectrically cooled, back-illuminated CCD camera (DU420 BV, Andor). Typical accumulation times were 20 s for Stokes spectra and 60 s for anti-Stokes spectra.

The one-color, transient resonance Raman spectra were measured as follows. First, an appropriate reference (Δt_{ref}) was determined by measuring a pump-only spectrum, a probe-only spectrum, and a set of (pump + probe) spectra at relatively long time delays; the reference Δt was chosen in a time delay region where the {pump-only + probe-only} − {pump + probe} yielded no measurable transient signal in either the Stokes or anti-Stokes portions of the Raman spectrum. For the experiments reported here, the Stokes transients utilized a $\Delta t_{ref} = 64$ ps and the anti-Stokes transients a $\Delta t_{ref} = -25$ ps. The anti-Stokes data were measured in groups of four spectra: (pump + probe) anti-Stokes spectra were measured at three consecutive Δt values, and then a (pump + probe) Δt_{ref} spectrum was measured. The groups of four spectra were collected in random order of time delay in order to avoid systematic errors. The transient spectra (Figure 1) were then obtained by subtracting the reference spectrum from its corresponding set of three pump−probe spectra, and then applying the background subtraction routine

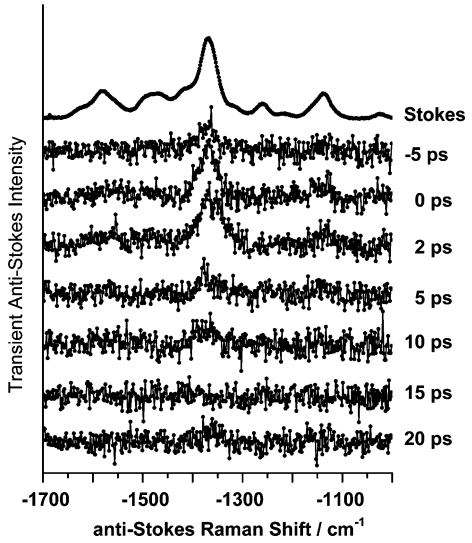

Figure 1. Transient anti-Stokes resonance Raman spectra of Fe^{II}OEP−2MeIm at the indicated time delays. The pump and probe wavelengths were 413 nm. Pump = 5.5 μJ/pulse; probe = 2.5 μJ/pulse. Transients were formed by subtracting reference spectra measured at $\Delta t_{ref} = -25$ ps. Baselines have been subtracted. The upper trace is a ground-state Stokes spectrum for reference.

in the *Origin 7.5* software package. The dynamics were measured several times. The Stokes transient spectra were measured in an analogous fashion, but with four Δt values for each reference spectrum; the stronger signal allowed shorter accumulation times. The kinetic traces derive from the peak intensities of the transient Raman spectra. Limited smoothing was performed by averaging three intensities at the peak position. The decay portions of the kinetic traces were fit with single-exponential functions using *Origin 7.5*.

Ultrafast Transient Absorption Spectroscopy. The femtosecond transient absorption experiments were performed at the Ohio Laboratory for Kinetic Spectrometry at Bowling Green State University. The details of the laser system and the experimental setup have been described in detail elsewhere.[34] Briefly, the output (800 nm, 100 fs, and 1 kHz) from a Spectra-Physics Hurricane was used to generate pump pulses at 400 nm and white-light continuum probe pulses (3 mm CaF_2 plate, 360−750 nm). The pump was chopped at 100 Hz, focused to ~2 mm at the sample, and overlapped with the probe in near-collinear geometry (~5°) with polarizations at magic angle. Signals were collected by a 400 μm optical fiber connected to a CCD spectrograph (Ocean Optics, PC 2000). The instrument response was 110 fs. The optical chopper, delay stage, and CCD spectrograph were controlled by LabView (National Instruments, Inc.) programs written by Ultrafast Systems, LLC. The sample was circulated under Ar gas pressure through a 1 mm flow cell using a micropump. The optical density of the sample was less than 1.0 at the excitation wavelength (402 nm). The final transient spectra are an average of three scans.

The continuum probe exhibited a positive chirp, that was corrected by fitting data at thirteen wavelengths to an empirical function [$y = A_2 + (A_1 - A_2)/(1 - (\lambda/\lambda_0)^P]$ chosen for goodness of fit across the experimentally measured range. $A_1 = 0.437\,74$; $A_2 = 1.154\,46$; $\lambda_0 = 393.937\,47$; $P = 7.652\,54$; root mean square (rms) deviation from the experimental values = 0.05. The (chirp-corrected) $\Delta t = 0$ at 426 nm was used for plotting the transients in the Soret band region. The $\Delta t = 0$ is chirp-corrected using this function for all of the kinetic traces analyzed and shown.

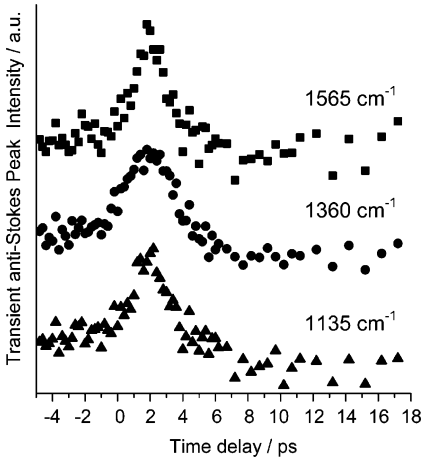

Figure 2. Kinetic traces were formed by averaging the three peak intensities for each band and then averaging these across multiple data sets. With the traces normalized to a peak value of 1, the rms error is 0.1, and the average absolute difference between the average and each individual data point is 0.08. No further processing was performed. Squares = ν_2, circles = ν_4, and triangles = ν_5.

Results

Ultrafast Time-Resolved Resonance Raman Spectroscopy. Excitation of the heme leads to the rapid increase in the anti-Stokes intensities of several vibrational modes. Figure 1 shows a set of transient anti-Stokes Raman spectra generated by exciting the molecule on the blue side of the Soret transition ($\lambda_{pump} = 413$ nm) and then probing at the same wavelength as a function of time delay. The most intense transient feature appears at 1360 cm^{-1} and is assigned to ν_4, a symmetric (A_{1g}) pyrrole breathing motion. This transition is the most intense in the Stokes spectrum as well. Two other peaks are weaker, but apparent. These bands at 1565 and 1135 cm^{-1} also grow in rapidly and decay completely by about $\Delta t = 10$ ps. The weak transient feature at 1565 cm^{-1} has been assigned to ν_2, an A_{1g} in-phase $C_\beta - C_\beta$ stretch.[35] The 1135 cm^{-1} band is most likely ν_5, a C_β-substituent mode.[36] CO photolysis experiments place ν_5 at 1112 cm^{-1}.[16,17] However, analysis of resonance Raman spectra of NiOEP assign a weak band at 1139 cm^{-1} to this motion.[36]

Figure 2 shows a kinetic analysis of the peak heights of the three bands discussed. Several observations can be made from these data. First, all three traces exhibit intensity well before $\Delta t = 0$. This is a consequence of the one-color, two-pulse method employed in these studies and is used to help evaluate the temporal characteristics of the incident pulse.[33] Both pulses are at 413 nm, so either can act as pump or probe. Nominally, this means that the signals will be symmetric about a minimum at $\Delta t = 0$. However, since the two beams impose different fluxes on the sample, the negative Δt changes are less intense than their positive counterparts. The ratio between the intensities of the "probe" and "pump" beams is about 0.4, so the dip position is shifted to slightly negative time delay (Figure 3).

The decay portions of these traces were fit with single exponentials (Table 1). The ν_4 and ν_5 bands decay with very similar kinetics, with 2.7 ± 0.2 and 2.9 ± 0.2 ps time constants, respectively. The ν_2 transient decays significantly more rapidly ($\tau = 1.6 \pm 0.2$ ps). The rises of the three bands have been estimated by simulating the data with the symmetric kinetics, weighted by 0.4 at negative time and convolved with a Gaussian pulse (fwhm = 600 fs). Figure 3 shows the result for ν_5, simulated with a 750 fs rise and the fit decay time. Clearly, the decay fits very well, and the rise kinetics are estimated fairly

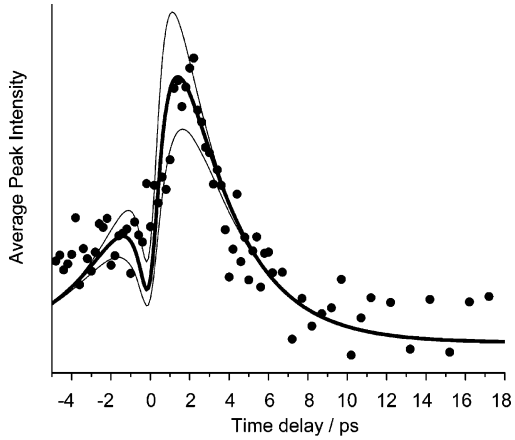

Figure 3. Simulated dynamics of ν_5. The symmetric single-exponential rise and single-exponential decay dynamics of the one-color TRARRS experiment was simulated. The best rise time (bold line) was found to be $\tau_{rise} = 750$ fs. Other rise times (500 fs, 1.0 ps; fine lines) were simulated to demonstrate accuracy. The decay was 2.8 ps, and a 600 fs Gaussian pulse width was convolved into the function. The ratio of probe to pump intensity was 0.4.

TABLE 1: Vibrational Dynamics in Photoexcited FeOEP−2MeIm

	anti-Stokes (TRARRS)			Stokes (TR^3S)	
vibrational mode	position/ cm^{-1}	τ_{RISE}[a]/ ps	τ_{DECAY}[b]/ ps	position/ cm^{-1}	τ_{BLEACH}[c]/ ps
ν_2	1565	0.65	1.6 ± 0.2	1580	2.0 ± 0.2
ν_3				1470	1.7 ± 0.2
ν_4	1360	0.75	2.7 ± 0.2	1362	2.2 ± 0.1
ν_{CH}				1260	2.4 ± 0.2
ν_5	1135	0.75	2.9 ± 0.2	1140	2.0 ± 0.2

[a] Determined from simulations of the kinetic traces in Figure 2 using the fit decay lifetime, a pump/probe relative flux of 0.4, and convolved with a 600 fs Gaussian laser pulse. [b] From fitting only the decay portions of the kinetic traces in Figure 2. [c] From fitting only the bleach recovery portions of the kinetic traces in Figure 5.

accurately. For comparison, simulations with rise times of 500 fs and 1.0 ps are shown as well. Similar traces for the ν_4 and ν_2 peaks gave rise times of 750 and 650 fs, respectively.

Complementary ultrafast time-resolved resonance Raman Stokes spectra ($\lambda_{pump} = \lambda_{probe} = 410$ nm) of Fe^{II}OEP−2MeIm are shown in Figure 4. The bleaching of the Stokes intensities at early times is apparent. As with the TRARRS spectra, bleach can be seen well before time zero as a consequence of the one-color, two-pulse method employed. The ν_4 (1362 cm^{-1}) band, strongest of the TRARR transient peaks, suffers the most loss of Stokes scattering intensity. Four other features are prominent, though weaker. A band at 1140 cm^{-1} is assigned to ν_5, the A_{1g} (C_β-substituent) stretch that appears in the ultrafast anti-Stokes spectra as well. The ν_2 mode (1580 cm^{-1}) also shows dynamics in both the Stokes and anti-Stokes spectra. The transients at 1260 and 1470 cm^{-1} do not have counterparts visible in the TRARR spectra. They are assigned to ν_{CH}, a symmetric CH_2 twist of the ethyl peripheral substituents, and ν_3, an A_{1g} ($C_\alpha-C_\beta$) symmetric stretching motion.

Figure 5 shows kinetic traces of the Stokes TR^3 intensities of the vibrational modes ν_2, ν_3, ν_4, ν_{CH}, and ν_5 at 1583, 1471, 1360, 1260, and 1140 cm^{-1}, respectively. Single-exponential decay fits are shown as well (Table 1). The bleach recovery signals exhibit similar kinetics. On average, they recover with a time constant of 2.1 ± 0.2 ps.

Ultrafast Transient Absorption Spectroscopy. Ultrafast TA spectroscopy with excitation on the blue side of the Soret band

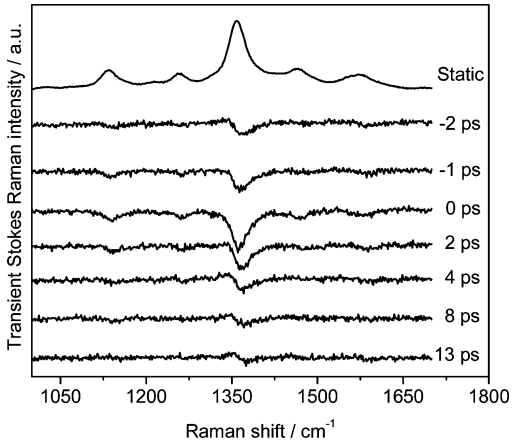

Figure 4. Transient Stokes resonance Raman spectra of Fe^{II}OEP−2MeIm at the indicated time delays. The pump and probe wavelengths were 410 nm. Pump = 5.5 μJ/pulse; probe = 2.5 μJ/pulse. Spectra are offset for clarity. Transients were formed by subtracting reference spectra measured at $\Delta t_{ref} = 64$ ps. The upper trace is a ground-state, static Stokes resonance Raman spectrum measured at 410 nm.

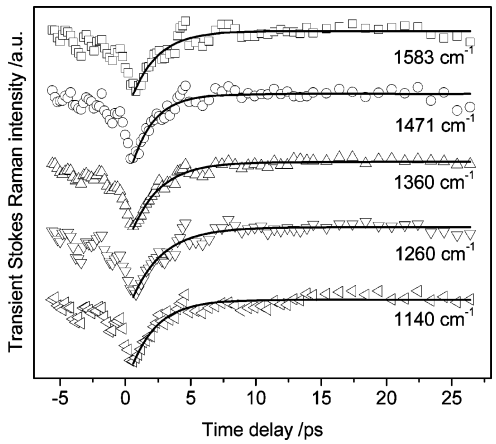

Figure 5. Kinetic traces were formed from TR^3 spectra (see Figure 4). Single-exponential decay results are collected in Table 1. Squares = ν_2, circles = ν_3, triangles = ν_4, inverted triangles = ν_{CH}, and rotated triangles = ν_5.

($\lambda_{pump} = 402$ nm; 110 fs instrument response) was performed to evaluate the behavior of the UV−vis absorption spectrum during the same time frame as the TR^3 and TRARR experiments. Figure 6 shows the evolution of the transient spectra in the Soret region to the red of the excitation pulse. Within the instrument response, a Soret-band bleach that corresponds to ground electronic-state depletion appears instantly. A broad, red-shifted transient absorption band rapidly blue-shifts and narrows until about $\Delta t = 2.5$ ps (Figure 6a). After that, a steady decrease in intensity and continued blue shift is observed (Figure 6b). The dynamics on the red side of the Soret are complete by about $\Delta t = 30$ ps.

Kinetic traces at several wavelengths (Figure 7) also show that evolution of the UV−vis absorption is quite complicated. The traces can be fit with exponential functions (Table 2); resulting time constants vary with wavelength. For example, from 430 to 480 nm, the τ_3 decay lifetime shortens monotonically from 12.1 ± 0.5 ps to 2.4 ± 0.3 ps. This sort of behavior is the hallmark of blue-shifting and/or narrowing of the underlying absorption bands that occurs on the time scale of the population changes.

Simulations of the Transient Absorption Dynamics. Simulations of the TA results were performed using a three-electronic-state model ($S_2 \rightarrow S_1 \rightarrow S_0^* \rightarrow S_0$). S_0^* represents

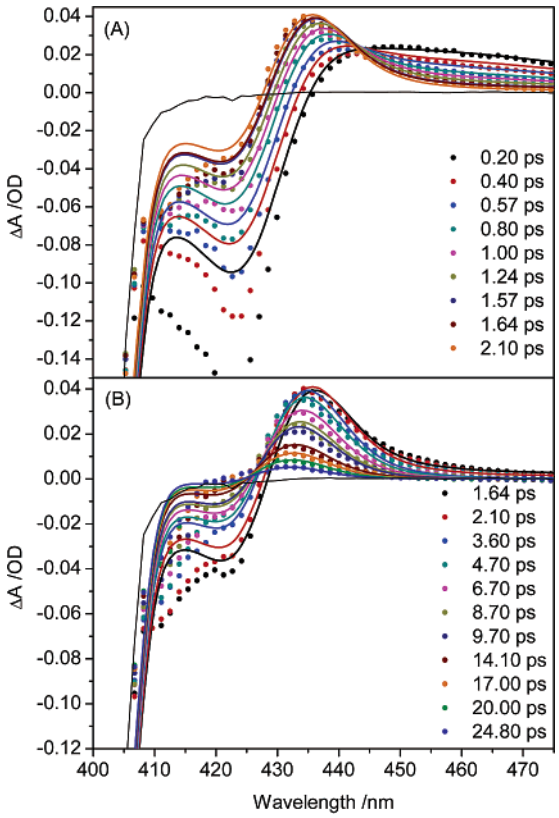

Figure 6. Transient absorption data (filled circles) and simulations (lines) for Fe^{II}OEP−2MeIm in CH_2Cl_2 at the indicated time delays. Pump = 402 nm, probe = white light continuum, and the instrument response = 110 fs. OD of the sample at 402 nm is <1.0. Panel A shows the fast dynamics associated with the first 2 ps after photoexcitation; panel B shows the slower dynamics on the 25 ps time scale. The simulation parameters are collected in Table 3. The large dip in the spectrum is a laser line artifact from the experiment (thin black line).

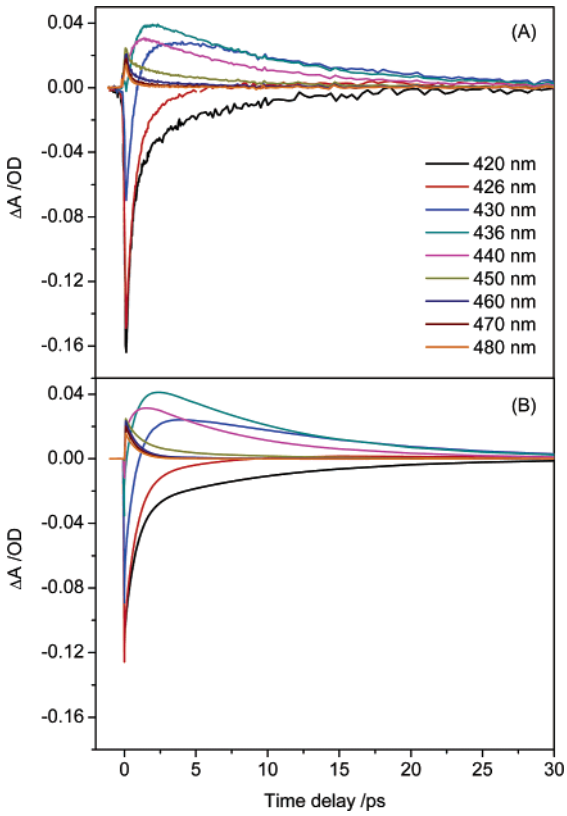

Figure 7. Kinetic traces of the TA signals for Fe^{II}OEP−2MeIm in CH_2Cl_2 at the indicated wavelengths. Pump = 402 nm, probe = white light continuum, and the instrument response = 110 fs. OD of the sample at 402 nm is <1.0. Traces are corrected for chirp in the probe. Panel A depicts the experimental measurement; panel B depicts the simulations (parameters collected in Table 3).

vibrationally excited, ground-state species newly created by IC from S_1. The line shapes (width, peak position) of both S_1 and S_0* were allowed to evolve in time; the S_2 and S_0 line shapes were static. In this model, S_2 and S_1 were treated as the Soret and Q-band excited electronic states, respectively.

Straightforward kinetic equations for the populations of S_2, S_1, and S_0* can be written

$$S_2(t) = S_2(0)\, e^{-t/\tau_2} \tag{1a}$$

$$S_1(t) = S_2(0)\frac{\tau_1}{\tau_2 - \tau_1}(e^{-t/\tau_2} - e^{-t/\tau_1}) \tag{1b}$$

$$S_0^*(t) = S_2(0)\left[\frac{\tau_1(1 - e^{-t/\tau_1}) - \tau_2(1 - e^{-t/\tau_2})}{\tau_1 - \tau_2}\right] \tag{1c}$$

where τ_2 and τ_1 are the lifetimes of the S_2 and S_1 states, respectively, and $S_2(0)$ is the fraction of molecules initially excited from S_0 by the incident light pulse, which is treated as a δ function here. The line shapes associated with these populations are given by single Gaussian functions for S_2 and S_1 of the form

$$G_2 = \frac{A_2}{\omega_2\sqrt{\pi/2}} \exp\left[-2\frac{(\bar{\nu} - \bar{\nu}_2)^2}{(\omega_2)^2}\right] \tag{2}$$

A_2 is the relative area, ω_2 is the width, and $\bar{\nu}_2$ is the peak energy of the $S_0 \rightarrow S_2$ absorption band; corresponding variables are used for the S_1 peak. For S_1, the width (ω_1) and center position ($\bar{\nu}_1$) were also allowed to vary in time exponentially.

TABLE 2: Kinetic Analysis for TA Data and Simulations

Exponential Fit to Experimental TA Measurements[a]

λ (nm)	A_1 (%), t_1 (fs)	A_2 (%), t_2 (ps)	A_3 (%), t_3 (ps)	A_4 (%), t_4 (fs)
420	−90, 433 ± 9	−10, 5.39 ± 0.14		
426	−90, 511 ± 33	−10, 1.58 ± 0.15		
430	−66, 615 ± 26	−11, 2.45 ± 0.77	23, 12.12 ± 0.50	
436	−57, 627 ± 8		43, 9.85 ± 0.08	
440	−43, 568 ± 15		57, 8.34 ± 0.08	
450			48, 6.67 ± 0.13	52, 361 ± 18
460			21, 4.82 ± 0.19	79, 312 ± 11
470			13, 3.09 ± 0.19	87, 244 ± 9
480			11, 2.44 ± 0.28	89, 245 ± 12

Exponential Fit to Simulated TA[a]

λ (nm)	A_1 (%), t_1 (fs)	A_2 (%), t_2 (ps)	A_3 (%), t_3 (ps)	A_4 (%), t_4 (fs)
420	−70, 661 ± 46	−30, 8.18 ± 0.97		
426	−22, 88 ± 20	−78, 1.13 ± 0.04		
430	−15, 38 ± 10	−63, 0.92 ± 0.02	22, 13.70 ± 0.54	
436	−60, 557 ± 58		40, 11.12 ± 1.22	
440	−56, 158 ± 23		44, 10.00 ± 0.98	
450			31, 6.06 ± 0.09	69, 932 ± 9
460			5, 5.06 ± 0.07	95, 818 ± 1
470			1, 4.14 ± 0.07	99, 805 ± 0
480			0.2, 2.86 ± 0.37	99.8, 800 ± 0

[a] $r^2 > 0.99$ for all fits except the last three experimental ones, which were 0.987, 0.979, and 0.966.

TABLE 3: Parameters Used in TA Simulations

	line shape parameters[a]					population dynamics
	$\bar{\nu}(0)/\mathrm{cm}^{-1}$	$\tau(\bar{\nu})$	$\omega(0)/\mathrm{cm}^{-1}$	$\tau(\omega)$	A	τ
S_0*	24500.0[b]	10 ps	1608[b]	8 ps	1155	
	23795.7		804		478	
S_0	24200.0		1340		−1155	
	23495.7		670		478	
S_1	22225		3000		800	800 fs
S_2					0	10 fs

[a] See text for details of the equations used to simulate the TA data. [b] The $\bar{\nu}(0)$ values for S_0* are red-shifted 300 cm^{-1} relative to the values for the thermal S_0 ground-state spectrum. The $\omega(0)$ values for S_0* are 1.2× the values for S_0.

The S_0 and S_0* line shapes were derived from nonlinear least-squares fitting of the experimental UV−vis spectrum with several Gaussian functions (*Origin v.7.5*, OriginLab Corp.) and then modeling with the minimum number required to give the basic Soret line shape. It was found that two Gaussians were sufficient to mimic most of the major features of the observed TA behavior (Table 3). G_0, the ground-state line shape, is static. However, G_0*(t) starts at $\Delta t = 0$ red-shifted and broadened relative to G_0 and shifts back to the G_0 values exponentially, with time constants of $\tau(\bar{\nu}_0$*) and $\tau(\omega_0$*).

This relatively simple line shape was chosen as an initial probe of the impact of the protein upon the static and dynamical line shape of the UV−vis absorption spectrum. It is clear that heme protein spectra are quite complex and inhomogeneously broadened and cannot be adequately modeled by simple Gaussians (see ref 37 for example). However, in our experiments, the FeOEP−2MeIm resides in a small-molecule solvent rather than in the highly anisotropic protein. The direct bonds between the heme and the protein at the periphery and at the iron are absent, as are the more indirect "through-space" interactions between the heme and the protein moieties and water molecules in the heme pocket. It is thus reasonable to begin with a relatively simple sum of Gaussians and test its ability to reproduce the observed data. In fact, a line shape of two Gaussians appeared to be sufficient for simulating the TA dynamics of the model compound in its small-molecule solvent.

The simulations and their comparison to the experimental data are presented in Figures 6−8. The S_2 state was assigned a very short lifetime ($\tau_2 = 10$ fs), on the basis of the observation that TA dynamics have been found to be very similar regardless of whether the Soret or the Q-band state is initially excited.[2,4,8] Given this, it was further assumed that the S_2 absorption does not contribute to the observed TA dynamics ($A_2 = 0$).

The four-orbital model of porphyrin UV−vis absorption attributes the ground-state spectrum (Soret and Q-band) to two pairs of transitions from the $a_{1u}(\pi)$ and $a_{2u}(\pi)$ occupied orbitals to a doubly degenerate $e_g(\pi^*)$ unoccupied orbital.[38] Promotion of one electron should thus lead to an S_1 state with an excited-state spectrum that has Soret and Q-band components, but shifted to the red, as the overall bond order of the macrocycle has been reduced. Holten and co-workers found that the S_1 excited-state absorption of a wide range of porphyrins is red-shifted relative to the ground-state absorption and is most likely $\pi-\pi^*$ in character.[39−41] A center position of 450 nm for the S_1 "Soret" absorption was found to be satisfactory. The lifetime of the S_1 state that best reproduced the TA data was found to

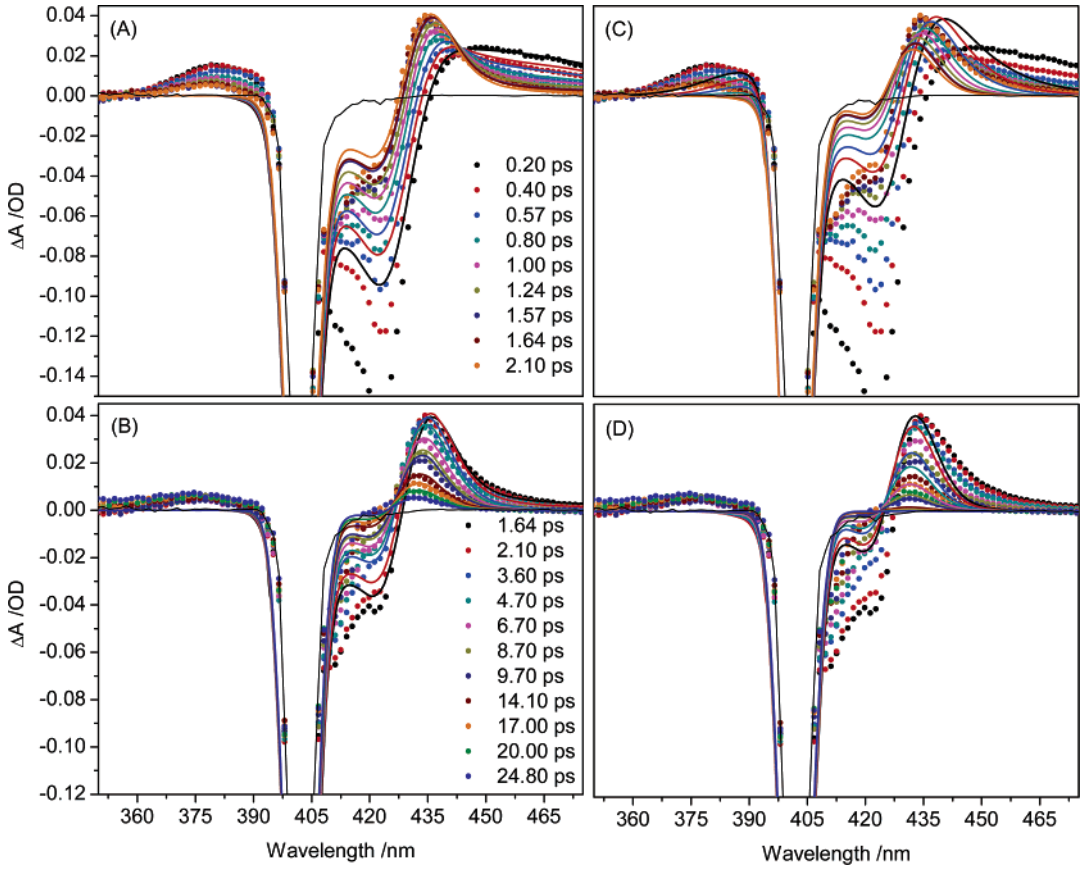

Figure 8. Transient absorption data (filled circles) and simulations (lines) for Fe^{II}OEP−2MeIm in CH_2Cl_2 at the indicated time delays. Left panels are the first 2 ps (panel A) and 25 ps (panel B) with simulations using the parameters in Table 3 (see Figure 6 legend for further details). Right panels are the first 2 ps (panel C) and 25 ps (panel D) with the same data, but simulations using time constants from ref 2 (S_0*: $\tau(\bar{\nu}_0$*) = 4 ps; $\tau(\omega_0$*) = 400 fs; initial $\bar{\nu}_0$* shift = −200 cm^{-1}; initial ω_0* broadening = 2.5×. S_1: $\tau_1 = 50$ fs).

be subpicosecond ($\tau_1 = 800$ fs), though values from 10 fs to 20 ps were tested. The contribution of S_1 transient absorption to the overall signal was also found to be very small. As mentioned above, the simulation includes the capacity for the S_1 state to evolve. However, it was found that no evolution of the S_1 line shape was required to mimic the major features of the TA signals. In the interest of minimizing adjustable parameters, then $\omega_1(t) = \omega_1(0) =$ constant and $\bar{\nu}_1(t) = \bar{\nu}_1(0) =$ constant.

The evolution of the $S_0^*(t)$ species dominated the TA signals. A wide range of values of the adjustable parameters $\bar{\nu}_0^*(0)$, $\tau(\bar{\nu}_0)$, $\omega_0^*(0)$, $\tau(\omega_0^*)$, and A_0^* was tested, and the parameters that best reproduced the data are collected in Table 3.

Discussion

Heme Electronic and Vibrational Dynamics in the Model Compound. This manuscript reports the electronic and vibrational dynamics of a symmetric, five-coordinate, high-spin model heme complex in an isotropic (to first-order) solvent environment. Complementary TA, TR^{3}S, and TRARRS experiments involve excitation of the blue side of the Soret (S_2) state and time-resolved monitoring of the evolution of the heme. The observed dynamics contain contemporaneous contributions from IC, IVR, and VER. Simulations of the evolving UV−vis absorption line width and position of the newly created ground-state heme reproduce the main features of both the TA spectra and the single-wavelength kinetic traces and provide a framework within which to interpret the time-resolved resonance Raman findings.

The electronic and vibrational dynamics of hemes have been the focus of numerous studies over more than 20 years. It is generally accepted that the ground electronic state is repopulated within about 5 ps of initial excitation, whether the pump laser is tuned to the Soret band (S_2) or the Q-band (S_1), and whether ligand photolysis is involved or not. However, broad consensus is still lacking for a model that describes how this rapid IC back to the ground state occurs.

The results presented here are consistent with a very rapid (sub-100 fs) $S_2 \rightarrow S_1$ transition, followed by a somewhat longer but still subpicosecond (800 fs) decay of S_1 to the ground electronic state. Given the rapidity of the IC processes, the amount of energy deposited in the vibrational manifold of the ground-state heme is quite significant. The newly created S_0^* absorption band appears to be broadened and shifted to lower energy. In our simulations, modest broadening of 20% and shifting of -300 cm^{-1} is sufficient to model the experimental data quite well. The narrowing and shifting to the room-temperature, thermal line shape of S_0 occurs on a 8−10 ps time scale and dominates the changes observed in the TA difference spectra. This process of shifting and narrowing reflects the vibrational relaxation of the heme, IVR, and VER on the ground-state surface.

Evaluation of the kinetic traces from the simulation, and comparison to the TA data, provides strong evidence for the accuracy of the main features of our simple kinetic model and the relatively simple line shape (Figure 7, Table 2). The overall pattern of the traces is nearly identical, and the lifetimes are quite similar as well. For example, in the traces from 430 to 480 nm, the behavior of component 3 is virtually identical in the measurements and the simulation. The lifetime changes from about 12−14 ps at 430 nm to 2−3 ps at 480 nm. It should be emphasized that only the time-dependent difference spectra were evaluated in optimizing the parameters. That is, the parameters were not adjusted to improve the fit with the kinetic trace analyses. Given this, the agreement between the data and the simulated kinetic traces is compelling.

The time-resolved Raman data are largely consistent with this picture as well. The anti-Stokes rise times are subpicosecond (~700 fs), indicating the recovery of the ground electronic state. The anti-Stokes signals decay with time constants of 1.5 to 3 ps, significantly shorter than the vibrational dynamics evident in the TA spectra and simulations. The most likely explanation is that the anti-Stokes signals are largely reflecting mode-selective IVR processes that rapidly redistribute the excess energy in a Boltzmann distribution, albeit at an elevated temperature. The anti-Stokes signals are quite weak, and it is likely that, once the excess energy is distributed over the >100 degrees of freedom of the heme, the vibrational excitation in the high-frequency region is below the detection threshold of our experiments. The narrowing and shifting of the UV−vis spectrum largely reflects the vibrational cooling of the heme to reach thermal equilibrium.

The line shapes of the resonance Raman bands change as well. Initially, they are broad, and they shift to lower frequencies as the system cools. This behavior offers significant possibilities for further study of the communication of the hot, non-Boltzmann heme with the rest of the macrocycle and the solvent bath (see, for example, refs 42 and 43).

This interpretation of rapid IVR (1−3 ps) and slower VER (~10 ps) is consistent with previous nanosecond transient resonance Raman studies of five-coordinate, high-spin hemes in a variety of solvent environments.[9−11] In these single-pulse studies, the anti-Stokes intensity is dependent upon the flux of the incident laser. As the flux increases, the heme is excited more frequently within a single pulse (50−200 excitation events per heme in a typical experiment), and a steady-state, non-Boltzmann distribution of vibrational energy associated with the ground electronic state is created and monitored with the transient anti-Stokes spectrum. One intriguing observation is that the distribution measured appears largely independent of the solvent. Very similar behavior is observed for the heme in Fe^{II} deoxyhemoglobin in the protein, Fe^{II} protoporphyrin IX in CTAB detergent micelles, and Fe^{II}OEP−2MeIm in CH_2Cl_2. It is reasonable, then, that the anti-Stokes signals reflect only intramolecular vibrational dynamics and that these are largely independent of the heme environment.

Comparison to Heme Protein Electronic Dynamics. Hemes are the active sites of a variety of critical biological systems, and the influence of the protein upon the behavior of the heme is a fundamentally important question to address. The study reported here upon the model FeOEP−2MeIm in CH_2Cl_2 provides a seminal opportunity to explore the impact of the protein upon the electronic and vibrational dynamics of the heme. The overarching observation that can be made is that the heme electronic and vibrational dynamics measured in isotropic solvent and protein environments exhibit more similarities than differences. That is, the impact of the protein upon heme dynamics seems to be rather subtle.

The data reported here are consistent with previously reported findings from heme proteins. A recent study of several heme proteins, and particularly of deoxymyoglobin, by Champion and co-workers proposes very short IC in five-coordinate, high-spin hemes, with sub-50 fs IC back to the ground state.[2] They pump in the Q-band and measure the TA in the Soret band region, and see most of the same features we observe.

Another recent TA study of deoxymyoglobin using ~70 fs pulses at 405 nm evaluated the Q-band and band III dynamics,

and concluded that there were no electronic dynamics by ~500 fs after excitation.[8] Vibrational dynamics associated with S_0* occurred on the 1's to 10's of picoseconds time scales and were modeled with an evolving line shape function as well. We find that the ~800 fs S_1 lifetime is required to fit the earliest dynamics (<2 ps; Figure 6A). This slight difference in S_1 lifetime might be due to the protein or to the excitation or probing conditions. In any case, our study supports the conclusions of both Ye et al.[2] and Kholodenko et al.[8] that the heme electronic dynamics are very rapid, certainly subpicosecond.

As a way to begin probing the influence of the protein, we imported the time constants for deoxymyoglobin of Ye et al. into our simulation model, with intriguing results (Figure 8C,D). The dynamics of the red side of the Soret were not satisfactorily reproduced at either early or late times. In addition to the sub-100 fs decay of S_1, Ye et al. propose a very broad, inhomogeneous S_0* ($2.5 \times S_0$) that evolves exponentially in both peak position and width, with lifetimes of 4 ps and 400 fs, respectively. With our simpler line shape function, these factors led to relatively shallow bleaches and difference spectra that narrow too quickly, particularly evident in the 435−465 nm region. Slowing down the narrowing process while maintaining the very short S_1 lifetime did not correct the discrepancies. In our simulations with the simpler line shape, the longer lifetime of the S_1 state along with the slower line width and position changes fits this region of the TA difference spectra much better.

These differences may have their origin in the environmental (e.g., protein versus CH_2Cl_2) impact upon the electronic state(s) and their dynamics, or may derive from imperfect models. It is clear from Figure 8 that our simulations do not represent a complete picture of heme vibronic dynamics. Though this region is difficult to assess because of the overlapping excitation line, the bleach at very early times appears too small relative to the positive signals. Perhaps more importantly, Figure 8A,B shows quite plainly that we do not adequately capture the behavior to the blue of the Soret band (~350−400 nm). Ye et al.[2] model the dynamics of this region more accurately at earlier times by using a very broad line width for S_0*. At long times, though, there is clearly a persistent transient absorption intensity to the blue of the initial bleach that neither our simulation nor that of Ye et al. picks up. Further study is clearly warranted to elucidate the origin of this transient difference signal.

The similarity of the TA results of FeOEP−2MeIm (in CH_2Cl_2, excited in the Soret) and deoxymyoglobin (in protein, excited in the Q-band) provides an excellent example of the robustness of heme photodynamics to the heme environment. That two fairly different simulations reproduce the data quite well suggests a subtle influence of the protein. In particular, the complexity of the static and dynamic line shape that seems required to simulate heme protein TA studies with high fidelity, but not for similarly high quality simulations in the nonprotein heme model system, is intriguing. Of course, detailed parallel comparative studies would enhance further exploration. However, it appears that the picture of heme dynamics, the five-coordinate, high-spin heme at least, is converging to one in which electronic dynamics are very rapid, and many of the TA and Raman observations are vibrational in origin. Actually, Holten and co-workers pointed out several years ago that the TA signatures of many metalloporphyrins are quite similar, with initially broad and red-shifted transient absorptions that relax on ~10 ps time scales.[39−41] The ubiquity of this behavior suggested to them that its origin could not be electronic but was rather a hallmark of porphyrin vibrational dynamics. Our findings are entirely consistent with this interpretation.

Not everyone shares this view, however. One of the earlier models of heme dynamics proposed multiple electronic decay pathways that repopulated S_0 on ~300 fs and ~3 ps time scales.[3,4] In the latest version of this model,[6] the photoexcited heme decays sequentially to an intermediate state called Hb_I* through a metal-to-ring charge-transfer event. The rapid back-charge transfer leads to Hb_{II}*, assigned to a vibrationally excited ground-state macrocycle with a d−d* excited metal ion center. The decay of Hb_{II}* back to the heme ground state then occurs on a 3 ps time scale. In a study of the band III region of deoxymyoglobin, the single wavelength kinetics are fit with two time constants (0.32 and 2.2 ps), and a single pathway decay through a putative intermediate state with a lifetime of about 3.4 ps is proposed. It is concluded that electronic decay is not subpicosecond.[7] These models were based all or in part upon global fitting procedures that omitted line shape evolution. The wavelength dependence of the kinetic traces suggest that such global fitting may not be appropriate.[2] The time constants can vary quite significantly across even relatively small regions of the UV−vis spectrum (Table 2). Neither the time-resolved anti-Stokes nor the TA simulations presented here provide evidence for a 3 ps electronic state lifetime.

Some potential complications from the concurrently changing transient absorption and resonance Raman spectra should be considered. The resonance cross section depends on the absorption strength as well as the vibrational level population and cross section. If the UV−vis spectrum is very broadened, the cross sections of both Stokes and anti-Stokes resonance Raman transitions may be lower than expected, depending upon the degree of broadening and the excitation wavelength. Reabsorption of the scattered light also will be affected by a changing absorption band but in the opposite manner, so that some fortuitous cancellation will occur. Ye et al. report a first-order attempt to examine the effect of the dynamical UV−vis absorption spectrum upon anti-Stokes signals, using several approximations and the Kramers−Kronig transformation.[2] Kozich et al. have developed a similar approach.[44] While the approximations (e.g., harmonic potential, Boltzmann distribution of vibrational energy even at very early Δt) limit quantitative applicability of this treatment to systems in vibrational and electronic flux, the results indicate that the vibrational lifetimes measured may be significantly different from their true values due to the evolving resonance conditions. At the moment, we attribute the anomalously long Stokes bleach recovery times to this effect, though this hypothesis remains to be tested. Currently, we are working on a way to more accurately probe these complicated, counteracting effects.

State Preparation, IC, and Vibrational Dynamics. One working hypothesis behind these studies is that the initial distribution of excess vibrational energy deposited in the ground electronic state from a photoexcited (or intermediate excited) electronic state, and the subsequent redistribution and relaxation dynamics, depend strongly upon (1) the total amount of excitation energy in the system, (2) the nature of the electronic excited state that couples to the ground state in the IC process, and (3) the intrinsic coupling of each mode to other molecular and solvent degrees of freedom. In practice, then, there is no single lifetime for a given vibrational mode.

The measured lifetime of a single mode reflects a complex set of dynamical processes. A fundamental, intrinsic $0 \leftarrow 1$ lifetime corresponds to the characteristic decay of the $v = 1$ vibrational level in the isolated, cold molecule. This τ_i^0 depends on the intramolecular coupling of mode i to other molecular degrees of freedom and is rather difficult to measure. In the

molecule at room temperature in solution, the measured lifetime τ_i is almost certainly quite different from τ_i^0. Intermolecular and intramolecular coupling to other motions will depend on the excess energy in the system, and the time-dependent populations of these other degrees of freedom strongly affect the vibrational dynamics. The non-Boltzmann distributions that may persist in a photoexcited molecule for several picoseconds may dramatically affect the measured lifetime in ways that are difficult to predict a priori.

In particular, these studies probe the dependence of heme vibrational dynamics upon the magnitude of the initial excess vibrational energy and the nature of the coupled excited state in IC. Comparisons of the TRARRS results to picosecond ligand−photolysis studies by Mizutani and Kitigawa provide insight into this fundamental issue. In those experiments, myoglobin with a CO ligand (Mb−CO) was photoexcited in the heme Q-band, and the resonance Raman Stokes and anti-Stokes spectra were measured as a function of time using λ_{probe} = 435 or 442 nm with ∼2−2.3 ps pulses.[16,17] Some very interesting behavior of the newly photolyzed, five-coordinate transient Mb* species was seen. Examination of the modes that appear in the transient anti-Stokes spectrum and their decay kinetics is illuminating.

Photolysis of the CO from MbCO rapidly (<1 ps) generated a vibrationally excited, five-coordinate, transient Mb* in its ground state but with significant population in ν_3 (1461 cm^{-1}), ν_4 (1360 cm^{-1}), ν_5 (1112) cm^{-1}, and ν_6/ν_{32} (779 cm^{-1}).[16,17] A ν_7 (669 cm^{-1}) band was also observed in some spectra.[17] In contrast, the early-time Fe^{II}OEP−2MeIm spectra exhibit significant intensity in ν_4, ν_2, and ν_5 (here at 1135 cm^{-1}), but ν_3, the peak at 1112 cm^{-1}, and ν_6/ν_{32} do not appear.

Within the framework discussed here, there are three possible sources for these differences. The spectra are measured at different positions within the UV−visible Soret absorption band, so resonance effects may be important. The environment (i.e., protein versus CH_2Cl_2) may play a significant role as well (vide infra). Here, though, we explore the interpretation that different subsets of modes are involved in IC for the two different processes. The coupling and accepting modes associated with IC lead to different initial vibrational energy distributions depending upon whether the excitation involves ligand photolysis. It is significant that the ν_4 transient is the most intense in both experiments. Clearly, this mode plays an important role in heme electronic dynamics.

The vibrational-state lifetimes differ slightly in the two TRARRS studies. The ν_4 transient decayed with time constants of 1.9 ± 0.6 ps (λ_{probe} = 436 nm)[16] and 1.1 ± 0.6 ps (λ_{probe} = 442 nm)[17] with CO photolysis. Both of these lifetimes are somewhat shorter than the 2.6 ± 0.2 ps measured with photoexcitation of Fe^{II}OEP−2MeIm. Clearly, this intriguing difference needs to be revisited in parallel experiments under identical conditions. ν_7 decayed with 1.9 ± 0.6 ps kinetics in the photolysis experiments when λ_{probe} = 442 nm but was not seen at 435 nm. We observed excitation in ν_7 as well, but it was considerably complicated by a solvent band; we were not confident in evaluating its kinetics unambiguously (not shown).

These differences are perhaps not surprising, as the two processes must necessarily participate in very different energy disposal processes. Mb−CO is a six-coordinate, low-spin heme in the ground state. Photoexcitation must ultimately result in the Fe ion becoming high-spin and moving out of the plane of the macrocycle. Photolysis also reduces the overall amount of energy that can wind up in the ground electronic state, because some of the excitation energy is required to break the Fe−C bond and some leaves with the newly photolyzed CO ligand. In the experiments by Mizutani and co-workers, this difference is compounded by their excitation in the lower-energy Q-band in the first place.

In contrast, Fe^{II}OEP−2MeIm is already a five-coordinate, high-spin heme with a domed conformation in the ground state. In addition, all of the energy from the absorbed photon is available to be deposited in the electronic ground state. The structural evolution of the two systems (e.g., the tuning modes) and the coupling of the excited states to the ground and any participating intermediate electronic states should differ and be reflected in different initial vibrational excited state distributions observed upon IC to the ground electronic state.[31,45] For example, Figure 2 indicates that ν_2, a mode that does not even appear in the CO photolysis transients, rises and decays faster than the other two modes seen in the TRARRS studies of Fe^{II}OEP−2MeIm. This indicates that ν_2 may be a strong accepting mode for IC in the nonligated heme and that it decays rapidly intramolecularly to populate other heme degrees of freedom.

The environment of the heme (i.e., protein versus CH_2Cl_2) may also play an important role in the vibrational dynamics measured by TRARRS. Recent molecular dynamics simulations by Straub and co-workers indicate that the details of the covalent attachment of the protein to the heme and the water and protein residues in the local heme pocket are highly influential in determining VER pathways and lifetimes.[22,27,28] The observation of vibrational excitation in ν_5, the C_β-ethyl mode, in our FeOEP−2MeIm studies indicates that energy flow does occur through the periphery in the model system. However, as discussed more fully in a previous section, the distribution of excess vibrational energy measured in five-coordinate, high-spin hemes in transient nanosecond anti-Stokes experiments is largely independent of the heme environment and most likely reflects intramolecular redistribution rather than VER.[9−11] Unfortunately, similar experiments on six-coordinate model systems are not available for comparison as yet. Thus, while the conclusions above are well-founded on the basis of the known differences between the five-coordinate, high-spin and six-coordinate, low-spin heme systems, parallel studies of analogous model systems will provide for more definitive conclusions.

Summary

The temporally overlapping, fast electronic and vibrational dynamics of the five-coordinate, high-spin heme in a nominally isotropic solvent environment has been studied for the first time with three complementary ultrafast techniques: transient absorption, time-resolved resonance Raman Stokes, and time-resolved resonance Raman anti-Stokes spectroscopies. The data are largely consistent with a picture in which the experimental observations are dominated by vibrational dynamics associated with an evolving ground-state species. Excitation into the blue side of the Soret band led to very rapid $S_2 \rightarrow S_1$ decay (sub-100 fs), followed by somewhat slower (800 fs) $S_1 \rightarrow S_0$* nonradiative decay. The initial vibrationally excited, non-Boltzmann S_0* state was simulated as shifted to lower energy by 300 cm^{-1} and broadened by 20%. On a ∼10 ps time scale, the S_0* state evolved into its room-temperature, thermally distributed S_0 profile. Comparisons of anti-Stokes mode intensities and lifetimes from TRARRS studies in which the initial excited state was prepared by ligand photolysis begin to paint a map of the pathways of vibrational energy flow in the ground electronic state and vibrational facilitation of the rapid IC

processes in these heme systems. While TA studies appear to be relatively insensitive to initial preparation of the electronic excited state, the subsequent vibrational dynamics are not. Clearly, more studies must be done before there is a full understanding of the photophysics and photochemistry in these systems and the fundamentally important influence of the protein upon them. However, these concerted electronic and vibrational experiments have provided an important first step in unraveling the vibrational participation in IC in hemes, the nature and pattern of heme vibrational dynamics established by photoexcitation, and the impact of the highly anisotropic protein environment upon them.

Acknowledgment. We thank the National Institutes of Health (GM056816) (M.C.S.) and the Provost's Opportunity Fund at Case Western Reserve University (M.C.S., T.C.G.). We also thank Stephan Brunello for his help in analyzing the time-resolved data.

References and Notes

(1) Li, P.; Sage, J. T.; Champion, P. M. *J. Chem. Phys.* **1992**, *97*, 3214.
(2) Ye, X.; Demidov, A.; Rosca, F.; Wang, W.; Kumar, A.; Ionascu, D.; Zhu, L.; Barrick, D.; Wharton, D.; Champion, P. M. *J. Phys. Chem. A* **2003**, *107*, 8156.
(3) Petrich, J. W.; Martin, J. L. *Chem. Phys.* **1989**, *131*, 31.
(4) Petrich, J. W.; Poyart, C.; Martin, J. L. *Biochemistry* **1988**, *27*, 4049.
(5) Franzen, S.; Bohn, B.; Poyart, C.; Martin, J. L. *Biochemistry* **1995**, *34*, 1224.
(6) Franzen, S.; Kiger, L.; Poyart, C.; Martin, J.-L. *Biophys. J.* **2001**, *80*, 2372.
(7) Lim, M.; Jackson, T. A.; Anfinrud, P. A. *J. Phys. Chem.* **1996**, *100*, 12043.
(8) Kholodenko, Y.; Volk, M.; Gooding, E.; Hochstrasser, R. M. *Chem. Phys.* **2000**, *259*, 71.
(9) Schneebeck (Simpson), M. C.; Vigil, L. E.; Ondrias, M. R. *Chem. Phys. Lett.* **1993**, *215*, 251.
(10) Simpson, M. C.; Peterson, E. S.; Shannon, C. F.; Eads, D. D.; Friedman, J. M.; Cheatum, C. M.; Ondrias, M. R. *J. Am. Chem. Soc.* **1997**, *119*, 5110.
(11) Loparo, J. J.; Cheatum, C. M.; Ondrias, M. R.; Simpson, M. C. *Chem. Phys.* **2003**, *286*, 353.
(12) Alden, R. G.; Chavez, M. D.; Ondrias, M. R.; Courtney, S. H.; Friedman, J. M. *J. Am. Chem. Soc.* **1990**, *112*, 3241.
(13) Alden, R. G.; Schneebeck (Simpson), M. C.; Ondrias, M. R.; Courtney, S. H.; Friedman, J. M. *J. Raman Spectrosc.* **1992**, *23*, 569.
(14) Lingle, R. J.; Xu, X.; Zhu, H.; Yu, S.-C.; Hopkins, J. B. *J. Phys. Chem.* **1991**, *95*, 9320.
(15) Lingle, R. J.; Xu, X.; Zhu, H.; Yu, S.-C.; Hopkins, J. B.; Straub, K. D. *J. Am. Chem. Soc.* **1991**, *113*, 3992.
(16) Mizutani, Y.; Kitagawa, T. *Science* **1997**, *278*, 443.
(17) Mizutani, Y.; Kitagawa, T. *Chem. Rec.* **2001**, *1*, 258.
(18) Alden, R. G.; Ondrias, M. R.; Courtney, S. H.; Findsen, E. W.; Friedman, J. M. *J. Phys. Chem.* **1990**, *94*, 85.
(19) Henry, E. R.; Eaton, W. A.; Hochstrasser, R. M. *Proc. Natl. Acad. Sci. U.S.A.* **1986**, *83*, 8982.
(20) Genberg, L.; Heisel, F.; McLendon, G.; Miller, R. J. D. *J. Phys. Chem.* **1987**, *91*, 5521.
(21) Genberg, L.; Richard, L.; McLendon, G.; Miller, R. J. D. *Science* **1991**, *251*, 1051.
(22) Bu, L.; Straub, J. E. *J. Phys. Chem. B* **2003**, *107*, 10634.
(23) Gu, Y.; Li, P.; Sage, J. T.; Champion, P. M. *J. Am. Chem. Soc.* **1993**, *115*, 4993.
(24) Ansari, A.; Berendzen, J.; Browne, S. F.; Frauenfelder, H.; Eben, I. E. T.; Sauke, T. B.; Shyamsunder, E.; Young, R. D. *Proc. Natl. Acad. Sci. U.S.A.* **1985**, *82*, 5000.
(25) Miller, R. J. D. *Annu. Rev. Phys. Chem.* **1991**, *42*, 581.
(26) Elber, R.; Karplus, M. *Science* **1987**, *235*, 218.
(27) Sagnella, D. E.; Straub, J. E. *J. Phys. Chem. B* **2001**, *105*, 7057.
(28) Bu, L.; Straub, J. E. *J. Phys. Chem. B* **2003**, *107*, 12339.
(29) Wang, Z.; Pakoulev, A.; Dlott, D. D. *Science* **2002**, *296*, 2201.
(30) Laubereau, A.; von der Linde, D.; Kaiser, W. *Phys. Rev. Lett.* **1972**, *28*, 1162.
(31) Kozich, V.; Werncke, W.; Dreyer, J.; Brzezinka, K.-W.; Rini, M.; Kummrow, A.; Elsaesser, T. *J. Chem. Phys.* **2002**, *117*, 719.
(32) Gunaratne, T. C.; Challa, J. R.; Simpson, M. C. *ChemPhysChem* **2005**, *6*, 1157.
(33) Gunaratne, T. C.; Milliken, M.; Challa, J. R.; Simpson, M. C. *Appl. Opt.* **2006**, *45*, 558.
(34) Gentili, P. L.; Danilov, E.; Ortica, F.; Rodgers, M. A. J.; Favaro, G. *Photochem. Photobiol. Sci.* **2004**, *3*, 886.
(35) Tsai, H.-H.; Simpson, M. C. *J. Phys. Chem. A* **2004**, *108*, 1224.
(36) Spiro, T. G.; Czernuszewicz, R. S.; Li, X.-Y. *Coord. Chem. Rev.* **1990**, *100*, 541.
(37) Srajer, V.; Shomacker, K. T.; Champion, P. M. *Phys. Rev. Lett.* **1986**, *57*, 1267.
(38) Gouterman, M. *J. Chem. Phys.* **1959**, *30*, 1139.
(39) Rodriguez, J.; Holten, D. *J. Chem. Phys.* **1989**, *91*, 3525.
(40) Rodriguez, J.; Kirmaier, C.; Holten, D. *J. Am. Chem. Soc.* **1989**, *111*, 6500.
(41) Rodriguez, J.; Kirmaier, C.; Holten, D. *J. Chem. Phys.* **1991**, *94*, 6020.
(42) Harris, C. B.; Shelby, R. M.; Cornelius, P. A. *Phys. Rev. Lett.* **1977**, *38*, 1415.
(43) Shelby, R. M.; Harris, C. B.; Cornelius, P. A. *J. Chem. Phys.* **1979**, *70*, 34.
(44) Kozich, V.; Werncke, W. *J. Mol. Struct.* **2005**, *735*−*736*, 145.
(45) Kozich, V.; Werncke, W.; Vodchits, A. I.; Dreyer, J. *J. Chem. Phys.* **2003**, *118*, 1808.